HAL
open science

NUMERICAL SIMULATIONS OF A 2D QUASI GEOSTROPHIC EQUATION

Jean-Paul Chehab, Maithem Trabelsi Moalla

To cite this version:

Jean-Paul Chehab, Maithem Trabelsi Moalla. NUMERICAL SIMULATIONS OF A 2D QUASI GEOSTROPHIC EQUATION. 2012. hal-00694541

HAL Id: hal-00694541

https://hal.science/hal-00694541v1

Submitted on 5 May 2012

HAL is a multi-disciplinary open access archive for the deposit and dissemination of scientific research documents, whether they are published or not. The documents may come from teaching and research institutions in France or abroad, or from public or private research centers.

L'archive ouverte pluridisciplinaire **HAL**, est destinée au dépôt et à la diffusion de documents scientifiques de niveau recherche, publiés ou non, émanant des établissements d'enseignement et de recherche français ou étrangers, des laboratoires publics ou privés.

NUMERICAL SIMULATIONS OF A 2D QUASI GEOSTROPHIC EQUATION

Jean-Paul Chehab

Laboratoire LAMFA, UMR CNRS 7352
Université de Picardie Jules Verne, Pôle scientifique
33, rue Saint Leu 80037 Amiens cédex, France, jean-paul.chehab@u-picardie.fr
& INRIA Nord-Europe, SIMPAF Project, Villeuneuve d'Ascq, France

Maithem Trabelsi Moalla

Unité de recherche : Multi-Fractals et Ondelettes
Faculté des Sciences de Monastir
Av. de l'environnement, 5000 Monastir, Tunisie

Abstract

This paper deals with the numerical simulations of the 2D generalized quasi geostrophic equation, where the velocity field is related to the solution θ by a rotation of Riesz transforms. Depending on the parameters of the problem, we present numerical evidences for long time behavior of the solution such as global existence effects or blow up in finite time.

1 Introduction

The quasi-geostrophic equations describe large-scale motions in the ocean and atmosphere at middle latitudes. Indeed, air that streams to the south is pushed east or west through Coriolis forces, creating a pressure gradient perpendicular to this motion. The resulting stationary state is called the geostrophic equilibrium. Then, describing the time dependence to lowest order, and since the vertical velocity has to be zero on the bottom of the ocean, or more generally on the lower boundary, the surface behavior can be written independently as a two dimensional equation. This gives rise to the "surface non dissipative quasi-geostrophic equations" see [8].

Here we focus on the 2D dissipative quasi-geostrophic equation, in a generalized version. Let $\mathbb{T}^2$ be the bi-periodic square $[0,1]^2$ of $\mathbb{R}^2$, let $0 < \alpha \leq 1$ be fixed and let f $\in L^2(\mathbb{T}^2)$ be a given scalar time independent function. We are looking for a real scalar function $\theta = \theta(t,x)$ defined on $\mathbb{R}_+ \times \mathbb{T}^2$ representing the temperature of the fluid and satisfying the following dissipative equation:

$$\partial_t\theta + \nu(-\Delta)^\alpha\theta + u.\nabla\theta = f, \quad x \in \mathbb{T}^2,\ t > 0, \tag{1}$$

and we suppose that the solution θ satisfies the following initial condition:

$$\theta(0,x) = \theta_0(x), \tag{2}$$

where $\nu > 0$ is the viscosity coefficient and $u = (u_1, u_2)$ is the velocity field which is related to the scalar θ by a rotation of Riesz transforms:

$$\begin{aligned} u &= Q_\beta(-\Delta)^{-\frac{1}{2}}\nabla^\perp\theta, && (3)\\ &= Q_\beta(-\partial_{x_2}(-\Delta)^{-\frac{1}{2}}\theta, \partial_{x_1}(-\Delta)^{-\frac{1}{2}}\theta). && (4)\end{aligned}$$

with

$$\mathbf{Q}_\beta = \begin{pmatrix} \cos\beta & -\sin\beta \\ \sin\beta & \cos\beta \end{pmatrix}.$$

Here $\beta \in [0, 2\pi)$ is a fixed parameter. We mention that when $\beta = k\pi$ we recover the usual 2D dissipative quasi geostrophic equation carrying the name of (SQG), for which the velocity is divergence free, and when $\beta \neq k\pi$ we recover the generalized 2D quasi geostrophic equation (GSQG). We notice that we consider periodic boundary conditions on $\mathbb{T}^2$.

In this paper, we aim at studying numerically the asymptotic behavior of the solutions, associated to both usual and generalized quasi geostrophic equation (SQG) and (GSQG). Part of the numerical simulations are made to confirm the results predicted by the theory, essentially that solutions to (SQG) globally exist for $\frac{1}{2} < \alpha \leq 1$, and that solutions to (GSQG) develop finite-time singularities for $\frac{1}{4} < \alpha \leq 1$. On the other hand, several numerical tests was performed on a large range of diffusion, viscosity and rotation parameters α, ν and β to depict key parameter dependence of the solutions, and particularly to control the impact of each parameter to guess the blow-up law.

This paper is organized as follows. In the second Section, we introduce the general framework and settings of our study, and we give some list of the existant theory. In section 3, we define the spectral discretization and we propose the numerical time schemes used for the numerical simulations. Then, we discuss their numerical properties in Subsection 3.2.1, namely the mean conservation property, and the numerical stability. Section 4, deals with the numerical simulations for both the usual and the generalized quasi-geostrophic equation.

2 Framework and settings

Before going ahead to exhibit our main results, we shall review the existing dynamic literature.

2.1 The usual quasi geostrophic equation(SQG)

In this section we only focus on the case $\beta = k\pi$, hence we take use of the divergence free property of the velocity field

$$div\ u = 0$$

that is exclusively verified in the non rotational case.

For the (SQG) equation, many studies were concerned with existence and regularity of quasi geostrophic solution, in the continuous case.
Global existence of classical solutions and uniqueness in weaker sense have been resolved for the (SQG) equation in the subcritical case $\alpha > \frac{1}{2}$, in [9] and [20] for instance. Some global well posedness results are also well known. We refer the reader to [14], [5] and [12] to more details. The critical case $\alpha = \frac{1}{2}$ was first dealt with by Constantin and al in [7] and later studied in [3], [4], [10], [15] and [26]. The harder case was the supercritical case $\alpha < \frac{1}{2}$ and it still a big challenge until now.
On the other hand, it is an open problem whether smooth initial data would blow up in finite time. Long time behavior of solutions to the dissipative (SQG) equation with forcing term, has been studied in Berselli [2], where the existence of the global attractor in L^2 space was proved in the critical case $\alpha = \frac{1}{2}$, and the existence of the weak global attractor was proved in the subcritical case $\alpha \in (\frac{1}{2}, 1)$. Whereas, Ning Ju solves the problem of existence of the global attractor in the

subcritical case with an affirmative answer in [15], see also [21] for a review of fundamental concept and techniques in analysis of infinite dimensional dynamical systems.
From the numerical point of view, Majda and Tabak in [18], first conducted numerical simulations and found that the non dissipative (SQG) equation with smooth initial data develop finite time singularities on $\nabla\theta$. However a more careful simulation later conducted in [8] and [19] revealed the absence of such singularity and attributed the observation in [18] to a growth of double exponential type.

2.1.1 Analytic properties for (SQG)

We point out that we consider the domain $\Omega = [0,1]^2$ with periodic boundary conditions. Let us recall Poincaré's inequality, for any mean zero function θ:

$$| (-\Delta)^{\frac{\alpha}{2}}\theta |_2^2 \quad \geq \quad C_0 \mid \theta \mid_2^2; \tag{5}$$

if λ_1 the first nonnegative eigenvalue of the operator $(-\Delta)$, with periodic boundary conditions, then $C_0 = \lambda_1^\alpha$.

Now, the following Lemma is proved.

Lemma 1 *We denote by $\bar{\theta} = \frac{1}{|\Omega|}\int_\Omega \theta dxdy$, the mean of the solution to (SQG), and by $\bar{f} = \frac{1}{|\Omega|}\int_\Omega f dxdy$, the mean of the external force f. Then $\bar{\theta}$ and $\bar{f}$ satisfy:*

1. $\frac{d}{dt}\bar{\theta} = \bar{f}$,
2. *if* $\bar{f} = 0$ *then* $\bar{\theta} = cte = \bar{\theta}_0$,
3. *if* $f = 0$ *then* $\lim_{t\to+\infty} \mid \theta - \bar{\theta} \mid_2 = 0$.

Proof:

1. it is obvious that, since we deal with periodic functions, and using (3) for $\beta = k\pi$, $(-\Delta)^\alpha\theta$ and $\nabla(u\theta)$ are mean zero functions, then we get the first property.
2. It follows promptly that if $\bar{f} = 0$ then $\bar{\theta} = cte = \bar{\theta}_0$
3. Furthermore, if $f = 0$ then $\theta - \bar{\theta}$ satisfies the following equation:

$$\partial_t(\theta) + \nu(-\Delta)^\alpha(\theta - \bar{\theta}) + u.\nabla(\theta - \bar{\theta}) = 0,$$

then, taking the inner product with $\theta - \bar{\theta}$, using the relation $\int \partial_t\theta(\theta - \bar{\theta})dx = \int \partial_t(\theta - \bar{\theta})(\theta - \bar{\theta})dx$,the Poincaré inequality and the fact that $\theta - \bar{\theta}$ is mean zero, we obtain:

$$\frac{1}{2}\frac{d}{dt} \mid \theta - \bar{\theta} \mid_2^2 + \nu C_0 \mid \theta - \bar{\theta} \mid_2^2 \leq 0,$$

hence,

$$| \theta - \bar{\theta} |_2^2 \leq e^{-2\nu C_0 t} \mid \theta_0 - \bar{\theta_0} \mid_2^2 \tag{6}$$

which goes to zero when t goes to infinity.

■

Concerning the energy point of view, it is well known from the work of S. Resnick [20] that $\forall T > 0,\ \theta_0 \in L^2,\ f \in L^1([0,T], L^2)$ the initial value problem (SQG) admits a solution,

$$\theta \in L^\infty([0,T], L^2) \cap L^2([0,T], H^\alpha) \tag{7}$$

that fulfill the energy estimate

$$\mid \theta(.,t) \mid_2^2 + \int_0^t \mid \Lambda^\alpha \theta(.,\tau) \mid_2^2 d\tau \leq \mid \theta(.,0) \mid_2^2 + \int_0^t \mid f(.,\tau) \mid_2 d\tau, \tag{8}$$

which leads to the energy conservation property in the continuous case when $f = 0$.

2.2 The generalized quasi geostrophic equation (GSQG)

In this section we shall focus on the case $\beta \neq k\pi$. Notice that the main problem which leads to the different theoretical study, is the loss of the divergence free property of the velocity field. Indeed, taking the divergence operator of equation (3), one can straightforwardly get

$$divu = \sin\beta(-\Delta)^{\frac{1}{2}}\theta$$

which equals zero only for $\beta = k\pi$. This lack, ensues automatically the loss of the numerical properties proved for the (SQG) in the sequent section.

Besides, the question of the global well posedness for the (GSQG) was first answered in the supercritical case in [17], the authors restricted their attention to radial solutions of constant sign, and they proved under some conditions on the initial data that the solution blows-up in finite time for $0 \leq \alpha < \frac{1}{4}$. We notice that they consider the whole domain $\mathbb{R}^2$ for their analysis and they prove that the blow-up occurs at the level of $\| \nabla\theta \|_\infty$. However, they mentioned that the restriction of α is just a limitation of their approach and conjectured that singularities exist for all supercritical range $0 \leq \alpha < \frac{1}{2}$.
It is obvious that radial solutions are steady state solutions for the usual inviscid (SQG) (i.e. $\nu = 0$) which is no longer the case for $\beta \neq k\pi$. Indeed, Dong and Li proved in [11] that smooth radial solution of the inviscid (GSQG) always develop gradient blow up in finite time. The criteria of blow-up is proved in the whole domain $\Omega = \mathbb{R}^2$ in [17], for the supercritical case, especially in the range $\alpha \in (0, \frac{1}{4})$ for smooth radial initial data that satisfies some properties. Besides, Balodis and Còrdoba showed in [1] the existence of singularities for the inviscid (GSQG) equation for $\beta = \frac{\pi}{2} + k\pi$. The authors obtained some new bilinear estimates for the Riesz transforms and used them to show the existence of singularities for general smooth initial data not necessarily radial, and without any restriction on the sign of θ.

3 Discretization schemes

3.1 Pseudo-spectral space discretization

Due to the periodic boundary conditions, the Fourier pseudo-spectral method appears to be suitable for the space discretization of the problem. We review in this section an essential description of this method, used in our computations.

We recall that for any periodic function f in $L^2(\Omega)$, f and all their derivatives take an expansion in terms of Fourier series according to:

$$f(x,y) = \sum_{k_1=-\infty}^{+\infty} \sum_{k_2=-\infty}^{+\infty} \hat{f}(k_1,k_2) e^{2i\pi k_1.x} e^{2i\pi k_2.y} \tag{9}$$

where (k_1, k_2) is the fourier discrete vector of $\mathbb{Z}^2$.
The Fourier coefficients $\hat{f}(k_1,k_2)$ are computed numerically in such a way, that $S_N f(x,y)$ interpolates f at the grid points (x_k, y_l), where $k,\ l = 0, ..., N-1$. They are defined by the relations:

$$S_N f(x_k, y_l) = \sum_{k_1=\frac{-N}{2}+1}^{\frac{N}{2}} \sum_{k_2=\frac{-N}{2}+1}^{\frac{N}{2}} \hat{f}(k_1,k_2) e^{2i\pi k_1.x_k} e^{2i\pi k_2.y_l}. \tag{10}$$

Then, using the discrete orthogonality we get inversely:

$$\hat{f}(k_1,k_2)) = \frac{4}{N^2} \sum_{k=\frac{-N}{2}+1}^{\frac{N}{2}} \sum_{l=\frac{-N}{2}+1}^{\frac{N}{2}} f(x_k, y_l) e^{-2i\pi k_1.x_k} e^{-2i\pi k_2.y_l}. \tag{11}$$

The further, serial pseudo-spectral algorithm being computed in practice ,by using fft routines.

Besides, using (11) and denoting by $k = (k_1, k_2)$, we define the derivative operators as follows:

$$\widehat{div(f)}(k) = ik.\hat{f}(k) \tag{12}$$

$$\widehat{\Lambda^\gamma f}(k) = \mid k \mid^\gamma \hat{f}(k), \tag{13}$$

where $\Lambda = (-\Delta)^{1/2}$.

3.2 The time marching schemes

For the time discretization, we propose five different schemes that will allow us not only to compare the numerical results for each of them, but also to validate the codes therein at the same time. We cite namely:

- the Forward Euler scheme,
- the linear Backward Euler scheme,
- the Sanz-Serna Cranck-Nickolson scheme,
- the Splitting scheme,
- the Runge-Kutta scheme.

We define hereafter the different schemes, and we review the existant properties therein. We also derive numerical analysis, for each one, namely concerning the mean conservation, and the numerical stability. In Section 4, we validate our results by implementing all these schemes.

3.2.1 The Forward Euler scheme

Let $\tau > 0$ be a fixed real, and set $t^n = n\tau$ for $n \in \mathbb{N}$. Then, we recursively construct elements θ^{n+1} which approches $\theta(t^{n+1})$ according to the first order convergence scheme:

$$\frac{\theta^{n+1} - \theta^n}{\tau} + \nu(-\Delta)^\alpha \theta^{n+1} + u^{n+1}.\nabla\theta^{n+1} = f. \tag{14}$$

Where θ^0 is an approximation of θ_0, and

$$u^{n+1} = Q_\beta(-\Delta)^{-\frac{1}{2}}\nabla^\perp\theta^{n+1}.$$

Existence, uniqueness, regularity results have been established in [23] for the infinite dimensional case. In the finite dimensional case an application of the fixed point Browder' Theorem, gives promptly the wished result. That is in particular, the sequence $(\theta^n)_n$ given by (14) is well defined for all $n \in \mathbb{N}$, see [22] for more details.

We begin by proving the following Proposition, which is a discrete version of Lemma 1:

Proposition 1 *$\bar{\theta^n}$ and $\bar{f}$ satisfy:*

1. $\bar{\theta^n} = n\tau\bar{f} + \bar{\theta^0}$
2. *if* $\bar{f} = 0$ *then* $\bar{\theta^n} = cte = \bar{\theta^0}$,
3. *if* $f = 0$ *then* $\lim_{n\to+\infty} \mid \theta^n - \bar{\theta^0} \mid_2 = 0$.

Proof:

1. equation (14) is written equivalently as follows:

$$\theta^{n+1} + \tau\nu(-\Delta)^\alpha\theta^{n+1} + \tau\nabla.(u^{n+1}\theta^{n+1}) = \tau f + \theta^n. \tag{15}$$

   Now getting the mean of equation (15), and using the fact that we treat periodic initial data, and that for these data derivatives are periodic and mean zero functions we get

$$\bar{\theta}^{n+1} = \bar{\theta}^0 + \tau\bar{f}. \tag{16}$$

   Hence recursively we get the wished result.

2. Since $\bar{f} = 0$ then the second point follows promptly from the first one.

3. If $f = 0$, then $\theta^{n+1} - \bar{\theta}^0$ satisfies:

$$\frac{(\theta^{n+1} - \bar{\theta}^0) - (\theta^n - \bar{\theta}^0)}{\tau} + \nu(-\Delta)^\alpha(\theta^{n+1} - \bar{\theta}^0) + u^{n+1}.\nabla(\theta^{n+1} - \bar{\theta}^0) = 0. \tag{17}$$

   Then getting the L^2 inner product of (17) with $\theta^{n+1} - \bar{\theta}^0$, and using the Poincaré inequality (5), and the fact that u^{n+1} is divergence free, we obtain:

$$< \frac{(\theta^{n+1} - \bar{\theta}^0) - (\theta^n - \bar{\theta}^0)}{\tau}, \ \theta^{n+1} - \bar{\theta}^0 > +\nu C_0 \mid \theta^{n+1} - \bar{\theta}^0 \mid_2^2 \leq 0. \tag{18}$$

Hence, due to the parallelogram identity we get:

$$\frac{1}{2}(\mid \theta^{n+1} - \bar{\theta^0} \mid^2 + \mid \theta^{n+1} - \theta^n \mid^2) + C_0 \nu\tau \mid \theta^{n+1} - \bar{\theta^0} \mid^2 \leq \frac{1}{2} \mid \theta^n - \bar{\theta^0} \mid^2 . \tag{19}$$

Then,

$$\mid \theta^{n+1} - \bar{\theta^0} \mid^2 \leq \frac{1}{1 + 2C_0\nu\tau} \mid \theta^n - \bar{\theta^0} \mid^2, \tag{20}$$

and since $\frac{1}{1+2C_0\nu\tau} < 1$, we obtain the result by a simple induction.

■

Now, we prove the unconditional stability of (14) in the sequent Proposition:

Proposition 2 *The forward Euler scheme (14), is unconditionally stable. Moreover, we have the following estimate:*

$$\mid \theta^{n+1} \mid_2^2 \leq \frac{1}{1 + \nu\tau C_0} \mid \theta^n \mid_2^2 + \frac{\tau}{4\nu C_0} \mid f \mid_2^2 . \tag{21}$$

Proof: taking the L^2 inner product of (14) with θ^{n+1}, leads to:

$$\begin{aligned} (\theta^{n+1} - \theta^n, \theta^{n+1}) &+ \nu\tau \mid (-\Delta)^{\frac{\alpha}{2}} \theta^{n+1} \mid_2^2 + \tau(u^{n+1}.\nabla\theta^{n+1}, \theta^{n+1}) \\ &= (\tau f, \theta^{n+1}). \end{aligned} \tag{22}$$

Then, applying the paralelogram inequality, Poincaré's inequality (5), and Young's inequality on (22), we get:

$$\mid \theta^{n+1} - \theta^n \mid_2^2 + \mid \theta^{n+1} \mid_2^2 - \mid \theta^n \mid_2^2 + 2\nu\tau C_0 \mid \theta^{n+1} \mid_2^2 \leq \frac{\tau^2}{2\varepsilon} \mid f \mid_2^2 + \frac{\varepsilon}{2} \mid \theta^{n+1} \mid_2^2, \tag{23}$$

for any $\varepsilon > 0$. Now, choosing $\varepsilon = 2\nu\tau C_0$ ensues:

$$\mid \theta^{n+1} \mid_2^2 \leq \frac{1}{1 + \nu\tau C_0} \mid \theta^n \mid_2^2 + \frac{\tau}{4\nu C_0} \mid f \mid_2^2 . \tag{24}$$

Let $\gamma = \frac{1}{1+\nu\tau C_0}$ which is a constant < 1, then, by a simple induction on (24) we obtain:

$$\mid \theta^n \mid_2^2 \leq \gamma^n \mid \theta^0 \mid_2^2 + \frac{\tau}{4\nu C_0(1-\gamma)} \mid f \mid_2^2 \tag{25}$$

$$\leq \gamma^n \mid \theta^0 \mid_2^2 + \frac{1 + \gamma\tau C_0}{4\nu^2 C_0} \mid f \mid_2^2 . \tag{26}$$

Hence, $\mid \theta^n \mid_2$ is uniformly bounded in L^2 and (14) is unconditionally stable. We point out that we have used the divergence free property of the velocity field.

■

3.2.2 The linearized Backward Euler scheme

This one, is a linearized Euler scheme which is given by:

$$\frac{\theta^{n+1}-\theta^n}{\tau}+\nu(-\Delta)^\alpha\theta^{n+1}+u^n.\nabla\theta^{n+1}=f. \tag{27}$$

The linear Backward Euler scheme is also a first order convergence scheme. Furthermore, analogous results concerning well posedness and global existence of solution to (27), are proved in [6], starting from an initial data $\theta^0\in H^\alpha$.
On the other hand, proving numerical stability and mean conservation properties of proposition 1 for (27) is identically the same task as for (14), owing to the canceling property of the nonlinear term, then it is omitted for conciseness.

3.2.3 The Sanz-Serna Crank-Nicolson scheme

For sake of precision, we implement this second order convergence' scheme, which reads:

$$\frac{\theta^{n+1}-\theta^n}{\tau}+\nu(-\Delta)^\alpha(\frac{\theta^{n+1}+\theta^n}{2})+(\frac{u^{n+1}+u^n}{2}).\nabla(\frac{\theta^{n+1}+\theta^n}{2})=f. \tag{28}$$

Obviously, this scheme satisfies as well the two first items of Proposition 1. Let us prove the third one. Indeed, since $f=0$, $\theta^{n+1}-\bar{\theta^0}$ satisfies:

$$\begin{aligned}\frac{(\theta^{n+1}-\bar{\theta^0})+(\bar{\theta^0}-\theta^n)}{\tau}+\nu(-\Delta)^\alpha(\frac{\theta^{n+1}-\bar{\theta^0}+\theta^n-\bar{\theta^0}}{2})\\ +(\frac{u^{n+1}+u^n}{2}).\nabla(\frac{(\theta^{n+1}-\bar{\theta^0})+(\theta^n-\bar{\theta^0})}{2})=0.\end{aligned} \tag{29}$$

Then, getting the inner product of (29) with $(\frac{\theta^{n+1}-\bar{\theta^0}+\theta^n-\bar{\theta^0}}{2})$, we obtain,

$$\frac{1}{2\tau}(\mid\theta^{n+1}-\bar{\theta^0}\mid_2^2-\mid\theta^n-\bar{\theta^0}\mid_2^2)+\frac{\nu}{4}\mid(-\Delta)^{\frac{\alpha}{2}}(\theta^{n+1}-\bar{\theta^0}+\theta^n-\bar{\theta^0})\mid_2^2=0. \tag{30}$$

It follows by Poincaré's inequality, that

$$\mid\theta^{n+1}-\bar{\theta^0}\mid_2^2+\frac{\nu\tau C_0}{2}\mid\theta^{n+1}-\bar{\theta^0}+\theta^n-\bar{\theta^0}\mid_2^2\leq\mid\theta^n-\bar{\theta^0}\mid_2^2, \tag{31}$$

and this means that $(\mid\theta^n-\bar{\theta^0}\mid_2^2)_n$ is a decreasing positive sequence, and hence convergent; $\exists l\geq 0\,/\lim_{n\to+\infty}\mid\theta^n-\bar{\theta^0}\mid_2^2=l$.
Then, since $\theta^n=cte$ is a solution to (28) with zero forcing term, and that for this case $l=0$, thus we get,

$$\lim_{n\to+\infty}\mid\theta^n-\bar{\theta^0}\mid_2^2=0,$$

and the third item of Proposition 1 is hence proved for the Sanz-Serna Crank-Nicolson scheme. ■

Remark 1 *An application of the fixed point Browder' Theorem in the finite dimensional case, gives as well that the sequence $(\theta^n)_n$ given by (28) is well defined for all $n\in\mathbb{N}$, by replacing only θ^{n+1} by $\frac{\theta^n+\theta^{n+1}}{2}$, see [22].*

However, it is shown hereafter, that the discretization (28) is not the better one due to his unfortunate local stability. Indeed, we only succeed to get a numerical stability in a range $[0, T^*]$ for a fixed T^*, given by the next Proposition:

Proposition 3 *For $f \in L^2([0,T^*], L^2)$ the Sanz-Serna scheme (28) is L^2-stable in any range $[0,T^*]$ for fixed T^*. Indeed*

$$| \theta^n |_2^2 \leq | \theta^0 |_2^2 + \frac{T^*}{2\nu C_0} | f |_2^2 . \tag{32}$$

Proof: taking the inner product of (28) with $(\frac{\theta^{n+1}+\theta^n}{2})$ we get

$$| \theta^{n+1} |_2^2 - | \theta^n |_2^2 + \nu\tau | (-\Delta)^{\frac{\alpha}{2}} \frac{\theta^{n+1}+\theta^n}{2} |_2^2 \leq \frac{1}{2\varepsilon} | \tau f |_2^2 + \frac{\varepsilon}{2} | \frac{\theta^n+\theta^{n+1}}{2} |_2^2 . \tag{33}$$

Then using Poincaré's inequality (5), and for $\varepsilon = \nu\tau C_0$, we infer that

$$| \theta^{n+1} |_2^2 + \frac{\nu\tau C_0}{2} | \frac{\theta^{n+1}+\theta^n}{2} |_2^2 \leq | \theta^n |_2^2 + \frac{\tau}{2\nu C_0} | f |_2^2 \tag{34}$$

Now let $T^* = n_0\tau$ a fixed finite time. Getting the sum $\sum_0^{n_0-1}$ of (34), and using the discrete Gronwall lemma we prove that $| \theta^n |$ is uniformly bounded according to the L^2 norm for any range $[0,T^*]$, and particularly we have,

$$\begin{aligned} | \theta^n |_2^2 + \frac{\nu\tau C_0}{2} \sum_{k=0}^{n_0-1} | \frac{\theta^{k+1}+\theta^k}{2} |_2^2 &\leq | \theta^0 |_2^2 + \frac{\tau(n_0-1)}{2\nu C_0} | f |_2^2 && (35) \\ &\leq | \theta^0 |_2^2 + \frac{T^*}{2\nu C_0} | f |_2^2 . && (36) \end{aligned}$$

■

Notice that comparing (36) and (26) gives an advantage to the forward and the linear backward euler schemes. Whereas, despite his unconditional stability, using the full implicit Euler scheme, one have to solve a large system of nonlinear equations. Then, the linearized scheme seems to be the perfect one at this stage. Hence, to take advantage of the improvement of the convergence order, without falling into numerical instabilities, we introduce the Strang Splitting scheme.

3.2.4 The Splitting scheme

The splitting approximation that we used here, consists on considering the diffusive and the convective parts separately, according to a Strang Formula, as follows.
Let us first define the operator L_t such that the solution of the linear diffusive part,

$$\begin{cases} \partial_t\theta + \nu(-\Delta)^\alpha\theta = 0, \\ \theta(0,.) = \theta_0(x), \end{cases} \tag{37}$$

writes

$$\theta(t,x) = L_t.\theta_0(x) = e^{-\nu t(-\Delta)^\alpha}\theta_0(x)$$

Accordingly, we first consider the diffusive part, and we look for a first intermediate half step solution, given by:

$$\theta^{n+\frac{1}{3}} = L_{\frac{\tau}{2}}\theta^n. \tag{38}$$

The second step of the Strang splitting, consists in taking the solution $\theta^{n+\frac{1}{3}}$ of the first step as an initial data to a Sanz-Serna Crank Nicolson discretization for the convective part, with a full time step τ. Namely, we look for a data $\theta^{n+\frac{2}{3}}$ solution of,

$$\frac{\theta^{n+\frac{2}{3}} - \theta^{n+\frac{1}{3}}}{\tau} + (\frac{u^{n+\frac{2}{3}} + u^{n+\frac{1}{3}}}{2}).\nabla(\frac{\theta^{n+\frac{2}{3}} + \theta^{n+\frac{1}{3}}}{2}) = f. \tag{39}$$

Finally, the third step reads:

$$\theta^{n+1} = L_{\frac{\tau}{2}}\theta^{n+\frac{2}{3}}. \tag{40}$$

Now, since we used a splitting scheme according to a Strang formula, and the corresponding sub-schemes (38)-(40) have all of them a convergence order $n \geq 2$, then the resulting discrete solution is some second order approximation of the solution to the system (1)-(2).

Proposition 4 *For the splitting scheme (38)-(40), $\bar{\theta^n}$ and $\bar{f}$ satisfy:*

1.
$$\bar{\theta^n} = L_{n\tau}\bar{\theta^0} + \tau\sum_{k=0}^{n} L_{(\frac{2k+1}{2})\tau}\bar{f}, \tag{41}$$

2. *if $\bar{f} = 0$ then $\bar{\theta^n} = L_{n\tau}\bar{\theta^0} \to 0$ when $n \to +\infty$,*

3. *if $f = 0$ then $\lim_{n\to+\infty} \mid \theta^n - \bar{\theta^n} \mid_2 = 0$.*

Proof:

1. from (39) we get $\bar{\theta^{n+\frac{2}{3}}} = \bar{\theta^{n+\frac{1}{3}}} + \tau\bar{f}$, so using (38) and (40) we deduce that,

$$\bar{\theta^{n+1}} = L_\tau\bar{\theta^n} + \tau L_{\frac{\tau}{2}}\bar{f}. \tag{42}$$

   A simple induction on (42) gives the desired relation.

2. If we replace $\bar{f} = 0$ in (41), we get $\bar{\theta^n} = L_{n\tau}\bar{\theta^0}$ which goes to zero when $n \to +\infty$, owing to the definition of L.

3. Now, suppose that $f = 0$ Eq.(39) rewrites:

$$\frac{(\theta^{n+\frac{2}{3}} - L_{(\frac{2n+1}{2})\tau}\bar{\theta^0}) - (\theta^{n+\frac{1}{3}} - L_{(\frac{2n+1}{2})\tau}\bar{\theta^0})}{\tau}$$
$$+(\frac{u^{n+\frac{2}{3}} + u^{n+\frac{1}{3}}}{2}).\nabla(\frac{\theta^{n+\frac{2}{3}} - L_{(\frac{2n+1}{2})\tau}\bar{\theta^0} + \theta^{n+\frac{1}{3}} - L_{(\frac{2n+1}{2})\tau}\bar{\theta^0}}{2}) = 0 \quad . \tag{43}$$

   Taking the L^2 inner product of (43) with $\frac{\theta^{n+\frac{2}{3}} - L_{(\frac{2n+1}{2})\tau}\bar{\theta^0} + \theta^{n+\frac{1}{3}} - L_{(\frac{2n+1}{2})\tau}\bar{\theta^0}}{2}$, it follows that:

$$\mid \theta^{n+\frac{2}{3}} - L_{(\frac{2n+1}{2})\tau}\bar{\theta^0} \mid_2^2 = \mid \theta^{n+\frac{1}{3}} - L_{(\frac{2n+1}{2})\tau}\bar{\theta^0} \mid_2^2 .$$

Besides, using this relation and (38), (40) we deduce that:

$$\begin{aligned}
\mid \theta^{n+1} - L_{(n+1)\tau}\bar{\theta^0} \mid_2 &= \mid L_{\frac{\tau}{2}}\theta^{n+\frac{2}{3}} - L_{(n+1)\tau}\bar{\theta^0} \mid_2 \\
&\leq \mid L_{\frac{\tau}{2}} \mid\mid \theta^{n+\frac{2}{3}} - L_{(\frac{2n+1}{2})\tau}\bar{\theta^0} \mid_2 && (44)\\
&\leq \mid L_{\frac{\tau}{2}} \mid\mid \theta^{n+\frac{1}{3}} - L_{(\frac{2n+1}{2})\tau}\bar{\theta^0} \mid_2 && (45)\\
&\leq \mid L_{\frac{\tau}{2}} \mid\mid L_{\frac{\tau}{2}}\theta^{n} - L_{(\frac{2n+1}{2})\tau}\bar{\theta^0} \mid_2 && (46)\\
&\leq \mid L_{\tau} \mid\mid \theta^{n} - L_{n\tau}\bar{\theta^0} \mid_2 . && (47)
\end{aligned}$$

Hence the result since $\mid L_\tau \mid < 1$.

■

Now, concerning the numerical stability point of view, the splitting scheme is unconditionally stable, owing to:

Proposition 5 *We suppose that θ satisfies $\int_\Omega \theta(t,x)dx = 0$, then the splitting scheme (38)-(40) is unconditionally stable. Moreover we have the following estimate:*

$$\mid \theta^{n+1} \mid_2 \leq \delta \mid \theta^n \mid_2 + \tau\sqrt{\delta} \mid f \mid_2, \tag{48}$$

where $\delta < 1$ is a contraction constant given in (53).

Proof: getting the L^2 inner product of (39) by $\theta^{n+\frac{2}{3}} + \theta^{n+\frac{1}{3}}$ leads to

$$\mid \theta^{n+\frac{2}{3}} \mid_2^2 - \mid \theta^{n+\frac{1}{3}} \mid_2^2 = \tau < f,\ \theta^{n+\frac{2}{3}} + \theta^{n+\frac{1}{3}} >_{L^2}, \tag{49}$$

then by Cauchy Schwarz we get

$$\mid \theta^{n+\frac{2}{3}} \mid_2 - \mid \theta^{n+\frac{1}{3}} \mid_2 \leq \tau \mid f \mid_2 . \tag{50}$$

On the other hand, referring to (38) and (40) and using the definition of the operator L_t, it becomes obvious that to get the uniform bound on $\mid \theta^{n+1} \mid_2$ we must contract the L^2 norm of the operator L_t. Indeed

$$L_t(\theta)(x,y) = \sum_{k_1,k_2\in\mathbb{Z}^2} \hat{\theta}_{k_1,k_2} e^{-\nu t\lambda^\alpha_{k_1,k_2}} e^{2i\pi k_1.x} e^{2i\pi k_2.y},$$

where λ_{k_1,k_2} are the eigenvalues of the operator $(-\Delta)^\alpha$. Then using the Parseval identity, we get

$$\mid L_{\frac{\tau}{2}}\theta \mid_2^2 = \sum_{k_1,k_2} \mid \hat{\theta}_{k_1,k_2} \mid^2 e^{-\nu\tau\lambda^\alpha_{k_1,k_2}}. \tag{51}$$

It follows, that for some mean zero periodic function θ, ($\lambda_{0,0} = 0$), we obtain:

$$\mid L_{\frac{\tau}{2}}\theta \mid_2^2 \leq e^{-\nu\tau\lambda^\alpha_{1,0}} \mid \theta \mid_2^2, \tag{52}$$

where $\lambda_{1,0}$ is the first nonnegative eigenvalue.
Hence, setting

$$\delta = e^{-\nu\tau\lambda^\alpha_{1,0}} < 1, \tag{53}$$

we ensure that $L_{\frac{\tau}{2}}$ is a contraction operator, and that

$$| L\theta |_2^2 \leq \delta | \theta |_2^2 . \tag{54}$$

Actually, we insert (54) in (38), (40) and then in (50), to get the wished result:

$$| \theta^{n+1} |_2 \leq \delta | \theta^n |_2 + \tau\sqrt{\delta} | f |_2,$$

and then follows promptly the unconditional stability of the splitting scheme.

■

Remark 2 *It would be possible to consider a first order convergence Strang splitting, if we have discretized the first and the third steps of the splitting according to a forward Euler scheme, and the unconditional stability would remain verified. Particularly, we get the following bound:*

$$| \theta^{n+1} |_2^2 \leq \frac{1}{1+\nu\tau C_0} | \theta^n |_2^2 + \frac{2\tau}{\nu C_0} | f |_2^2 .$$

Remark 3 *We emphasize that the solution θ^{n+1} obtained by the four schemes, fulfill the previous numerical properties, only for the usual quasi geostrophic equation (SQG), due to the divergence free velocity field. Furthermore, owing to the linearity of the spectral discretization, the properties proved for the semi-discretization in time, still available for the full one.*

In order to get a full discretization of the equation (1), we shall go back to the pseudo- spectral discretization of the previous subsection. For instance, we insert (12) and (13) on (14), and this leads to the full discretized scheme:

$$\widehat{\theta^{n+1}}(Id + \nu\tau | k |^{2\alpha}) = (\widehat{\theta^n} + \tau\widehat{f^{n+1}}) - i\tau k.(\widehat{u^{n+1}.\theta^{n+1}}). \tag{55}$$

Where $u^{n+1} = \mathcal{F}^{-1}(\widehat{u^{n+1}})$ and

$$\widehat{u^{n+1}} = (-i\frac{k_2}{| k |}\widehat{\theta^{n+1}}, i\frac{k_1}{| k |}\widehat{\theta^{n+1}}). \tag{56}$$

Doing the same for the different time schemes introduced in this section, we get three other full discretizations of (1).

3.2.5 The Runge-Kutta scheme

For an accurate simulation of the blow-up in the case of the (GSQG) equation, we considered this third order convergence scheme introduced by Driscoll in [13]. In that paper, the author proposed a composite method in which different integrators are used for different parts of Fourier Space: a standard Runge-Kutta fourth order integrator (RK4) at the lowest wave numbers and stiffly stable, and a linearly implicit third order Runge-Kutta at high wave numbers where the explicit method fails.
Noting by λ the matrix of the linear term which is here the fractional Laplacian, and $f(\theta(t))$ is the nonlinear term which is here the convective term, the equation under consideration is then

$$\dot{\theta(t)} = f(\theta(t)) + \lambda\theta(t) \tag{57}$$

The method consists on partition (57) into

$$\dot{\theta(t)} = f(\theta(t), z(t)) + \lambda\theta(t) \tag{58}$$

$$\dot{z(t)} = g(\theta(t), z(t)). \tag{59}$$

Then the scheme reads:

$$K_1 = \theta^n$$

$$\tilde{K_1} = z^n$$

$$K_2 = (1 - \frac{1}{3}\tau\lambda)^{-1}(\theta^n + \frac{1}{2}\tau f(K_1, \tilde{K_1}) + \frac{1}{6}\tau\lambda K_1)$$

$$\tilde{K_2} = z^n + \frac{1}{2}\tau g(K_1, \tilde{K_1}),$$

$$K_3 = (1 - \tau\lambda)^{-1}(\theta^n + \frac{1}{2}\tau f(K_2, \tilde{K_2}) + \frac{1}{2}\tau\lambda K_1 - \tau\lambda K_2)$$

$$\tilde{K_3} = z^n + \frac{1}{2}\tau g(K_2, \tilde{K_2})$$

$$K_4 = (1 - \frac{1}{3}\tau\lambda)^{-1}(\theta^n + \tau f(K_3, \tilde{K_3}) + \frac{2}{3}\tau\lambda K_3)$$

$$\tilde{K_4} = z^n + \tau g(K_3, \tilde{K_3})$$

$$\theta^{n+1} = \theta^n + \frac{1}{6}\tau[f(K_1, \tilde{K_1}) + f(K_4, \tilde{K_4}) + \lambda(K_1 + K_4)]$$
$$+\frac{1}{3}\tau[f(K_2, \tilde{K_2}) + f(K_3, \tilde{K_3}) + \lambda(K_2 + K_3)],$$

$$z^{n+1} = z^n + \frac{1}{6}\tau[g(K_1, \tilde{K_1}) + g(K_4, \tilde{K_4})] + \frac{1}{3}\tau[g(K_2, \tilde{K_2}) + g(K_3, \tilde{K_3})]$$

We emphasize that this method is a third order stable method, and that his constant error is close to the best achievable, and that our choice is essentially made for optimum performance, especially to get the exact blow-up time in the most perfect manner, and that results obtained by the Driscoll scheme, agrees with those obtained by the linear backward Euler one, for instance.

4 Numerical results

4.1 Aims

Our aim in this paper is to capture some theoretical properties, yet proved in previous works, by numerical simulations on (SQG), namely the global existence effect, and the L^2 norm conservation property for $\beta = k\pi$. Then the first part of numerical computations will be devoted to the validation of our codes, by implementing them at the same time, and comparing the results therein.
On the other hand, we aim to explore the (GSQG) equation, particularly, we discuss the formation of singularities at $\beta \neq k\pi$, for various values of the diffusion and the viscosity parameters α and ν.

Particularly, we intend to study the interaction of these parameters to get a law which controls the blow-up criteria, that will be discussed in the last part of this section.
Besides, we emphasize that our simulations are performed in the torus $\mathbb{T}^2$, unlike the paper of José and Lie [17], in which the authors considered the whole space $\mathbb{R}^2$ and this gives us a good opportunity of comparison.

4.2 Numerical simulations for SQG

We choose Matlab ® for the implementation of our codes taking advantage of the built-in FFT commands.

Besides, we notice that we used two different methods for the space discretization: the Fourier pseudo-spectral method and the finite differences one (whose results are not reported here), this last one being first used for validating the Fourier code; however, we point out that the use of the finite differences method allows us to explore new frameworks. Indeed, this code is let to later work to get numerical simulation for homogeneous or open boundary conditions. In this paper we, concentrate only on the spectral code.
To validate our codes, three main tests were implemented using the previous discretizations, according to (14), (28) and (38)-(40) schemes, starting with the initial data:

$$\theta_0(x,y) = \sin(2\pi x)\sin(2\pi y).$$

At first, let us check the output of our code when computing the approximation of a real function θ given by:

$$\theta(x,t) = \sin(2\pi x)\sin(2\pi y)\exp(\sin t) = \theta_{exact} \tag{60}$$

which is a solution of (1) according to the external force

$$f = \mathcal{F}^{-1}(\cos t\hat{\theta} + \nu \mid k \mid^{2\alpha} \hat{\theta} + \exp(\sin t)\widehat{u_0.\nabla\theta}). \tag{61}$$

Where u_0 is the velocity field corresponding to θ_0 according to the formula (3) with $\beta = 0$.
The subsequent figures represent respectively, a mean square fitting of the L^2- norm and the $L^\infty-$ norm convergence errors. These simulations are results of the forward Euler, the Sanz-Serna and the Splitting schemes with different time steps Δt. The plots for $N = 32$, $\beta = 0$, $\nu = 0.0001$ and $\alpha = 1$ are given in Figure(1), Figure(2) and Figure(3).

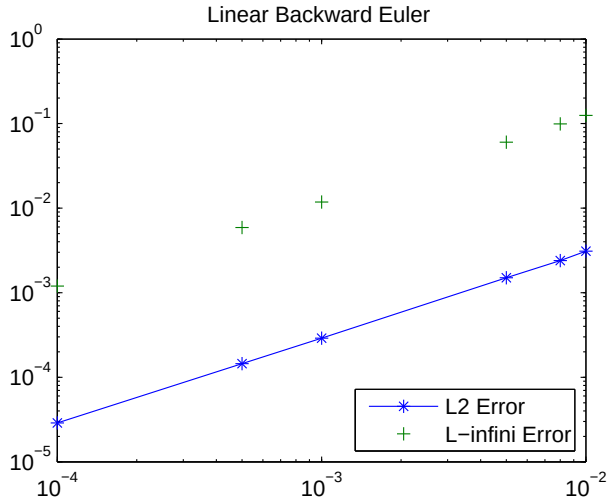

Figure 1: The evolution of the L^2 error norm and the L^∞ error norm Vs τ for an exact solution according to the linearized backward Euler scheme

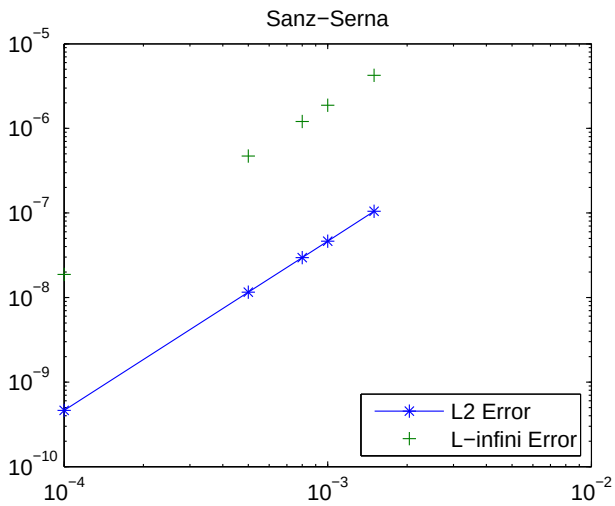

Figure 2: The evolution of the L^2 error norm and the L^∞ error norm Vs dτ for an exact solution according to the Sanz-Serna Crank-Nicolson scheme

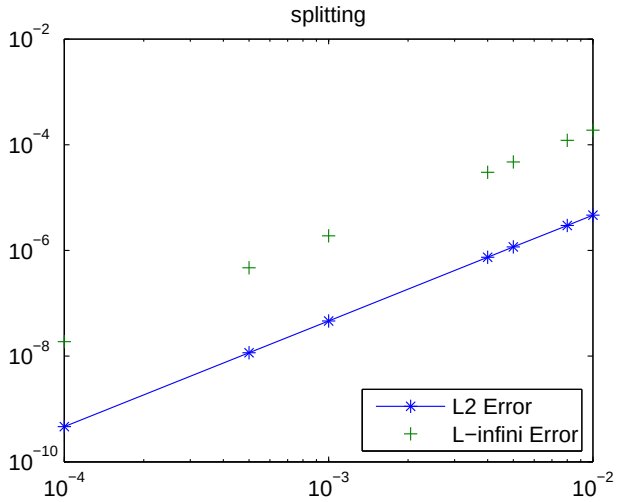

Figure 3: The evolution of the L^2 error norm and the L^∞ error norm Vs τ for an exact solution according to the splitting scheme

Hence, we confirm by the previous figures that the error corresponds to a first order convergence scheme, for Figure.(1), and to second order convergence schemes for Figure.(2) and Figure.(3). Indeed, the slopes of the three curves are given respectively by:

$$a_1 = 1.036 \tag{62}$$

$$a_2 = 2.0018 \tag{63}$$

$$a_3 = 2.0015, \tag{64}$$

and this contribute to confirm the validity of the codes. Next, we show a comparison between the three curves in Figure (4)

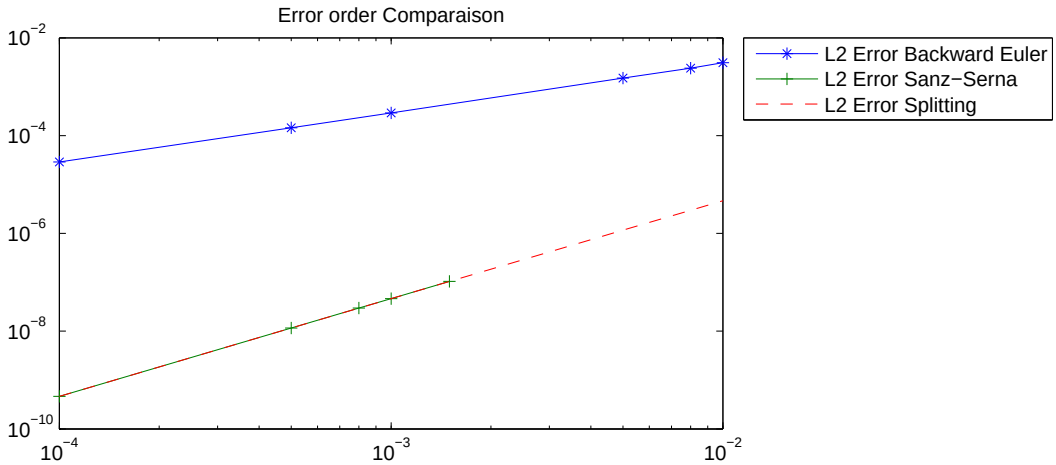

Figure 4: A comparison between the three schemes of the L^2 norms Vs τ.

Keeping the same previous parameters α and ν unchanged, we also run numerical simulations of dissipative (SQG) with various initial data and external forces, to display results of proposition 1

using the linearized backward Euler scheme in Figure(5), the splitting scheme in Figure(6) and the Sanz-Serna scheme in Figure(7). We emphasize that this last test were implemented for $\nu = 1$ for sake of stability. We ran respectively the cases $f = 2\theta^0$, $f = 1$ and $f = 0$ emanating from the initial data $\theta^0 = \sin(2\pi x)\sin(2\pi y)$ for $N = 64$ and $\tau = 10^{-4}$.

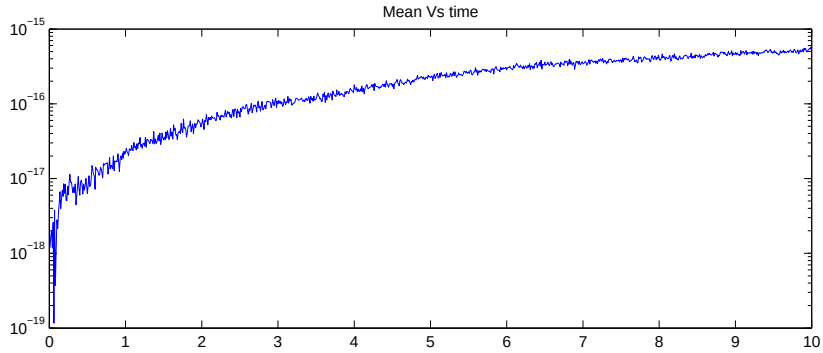

Figure 5: The mean of θ Vs time according to the external force $f = 2\theta_0$ using the linearized backward Euler scheme

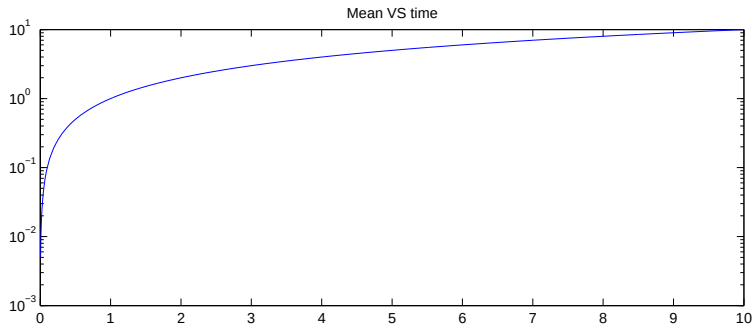

Figure 6: The mean of θ Vs time according to the external force $f = 1$ using the splitting scheme

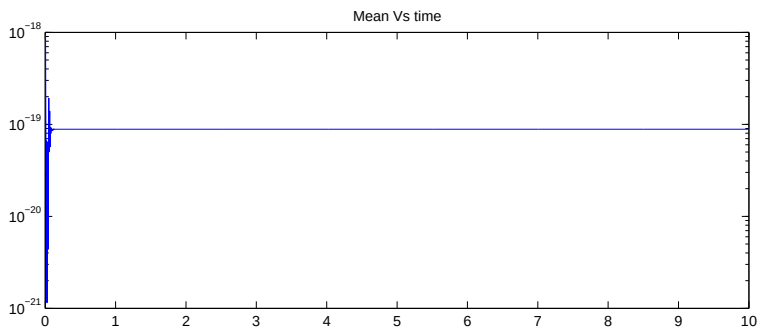

Figure 7: The mean of θ Vs time according to the external force $f = 0$ using the Sanz-Serna Crank-Nicolson scheme

Now we move on towards the third step of validation, to confirm the global existence results of [6] for instance. For that purpose, we plot the L^2 norm, and the contour lines of the solution to the dissipative (SQG) for $\alpha = 0.67 \geq \frac{2}{3}$, using the full implicit Euler scheme. By these simulations, we observed that this norm became bounded for $t \geq T^*$ for some fixed time T^*as illustrated in Figure(8) and Figure(10).

At this point, we underline that for these simulations, we have changed the choice of the initial data θ^0 and the external force F, to restrict ourself only to periodic data that belongs to L^2 and eventually to L^p for $p \leq \frac{2}{1-\alpha}$, and no more regular, to catch exactly results of the main Theorem in [6]. So let $\theta^0 = \sqrt{\sin(2\pi x(1-x))\sin(2\pi y(1-y))}$, and let $F = 2\theta^0$. The simulations are represented comparatively for the initial and the final step of plotting, in Figure(8) and Figure(9), giving respectively the behavior of the solution, and its contour lines. Whereas in Figure(10) we draw the solution' L^2 norm accordingly to $F = 2\theta^0$ and for $F = 0$, then the convergence to the global attractor is obviously faster in the second case, owing to the higher regularity of the external force. This is shown in figure (10):

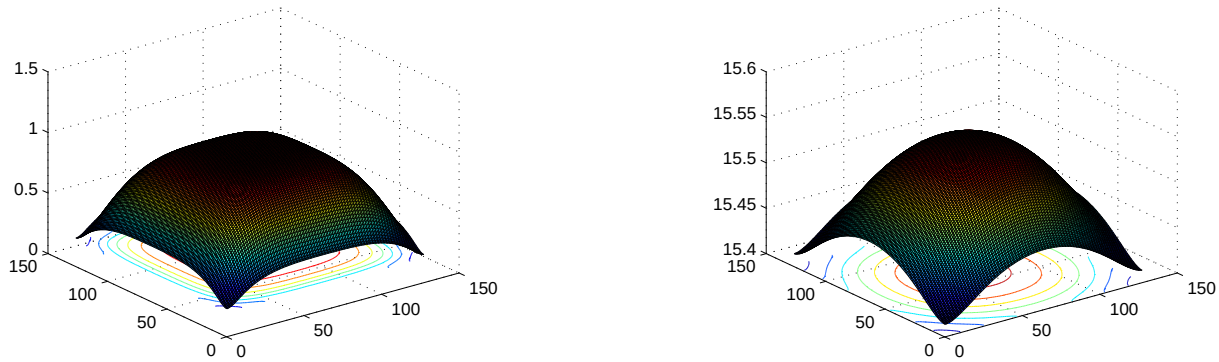

Figure 8: The evolution of the behavior of an L^2 initial data θ^0, with $f = 2\theta_0$ according to a full implicit Euler scheme

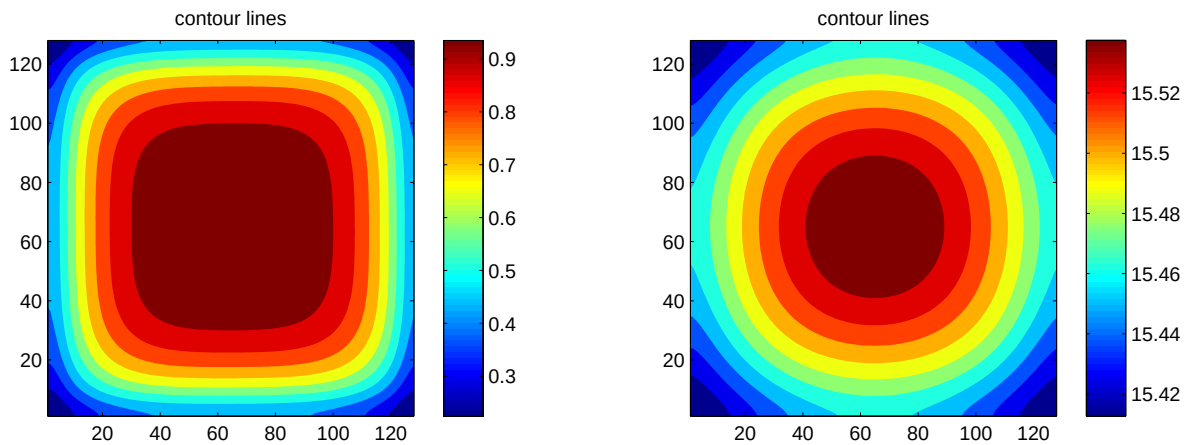

Figure 9: The evolution of the contour lines of an L^2 initial data θ^0, with $f = 2\theta_0$ according to a full implicit Euler scheme.

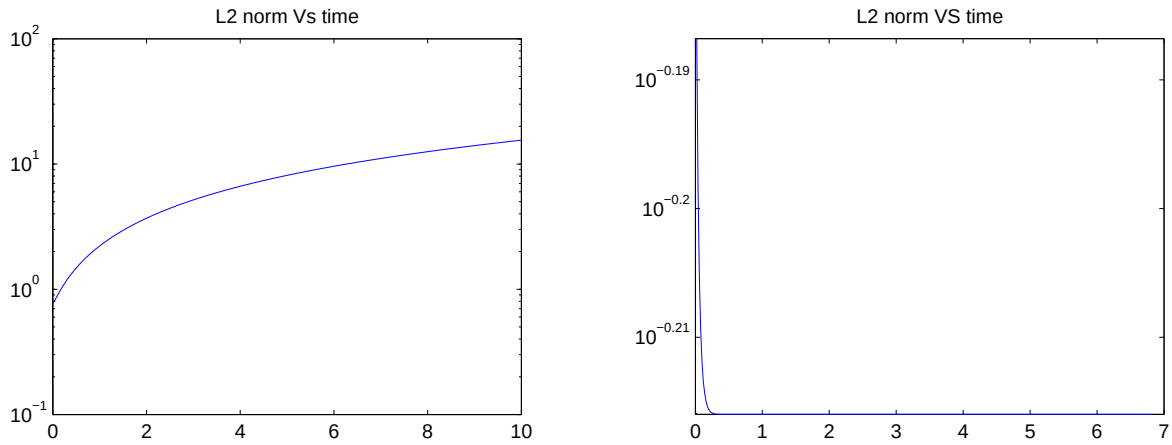

Figure 10: Global existence starting from an L^2 initial data θ^0, first with $f = 2\theta_0$ and second for $f = 0$ according to a full implicit Euler scheme.

Originally, numerical simulations denied the critical behavior at $\alpha = \frac{2}{3}$, and even at $\alpha = \frac{1}{2}$. In fact, this can be deduced by the convergence to the global behavior of the discrete solution to the forward Euler scheme at $\alpha = \frac{1}{2}$, in Figure(11).

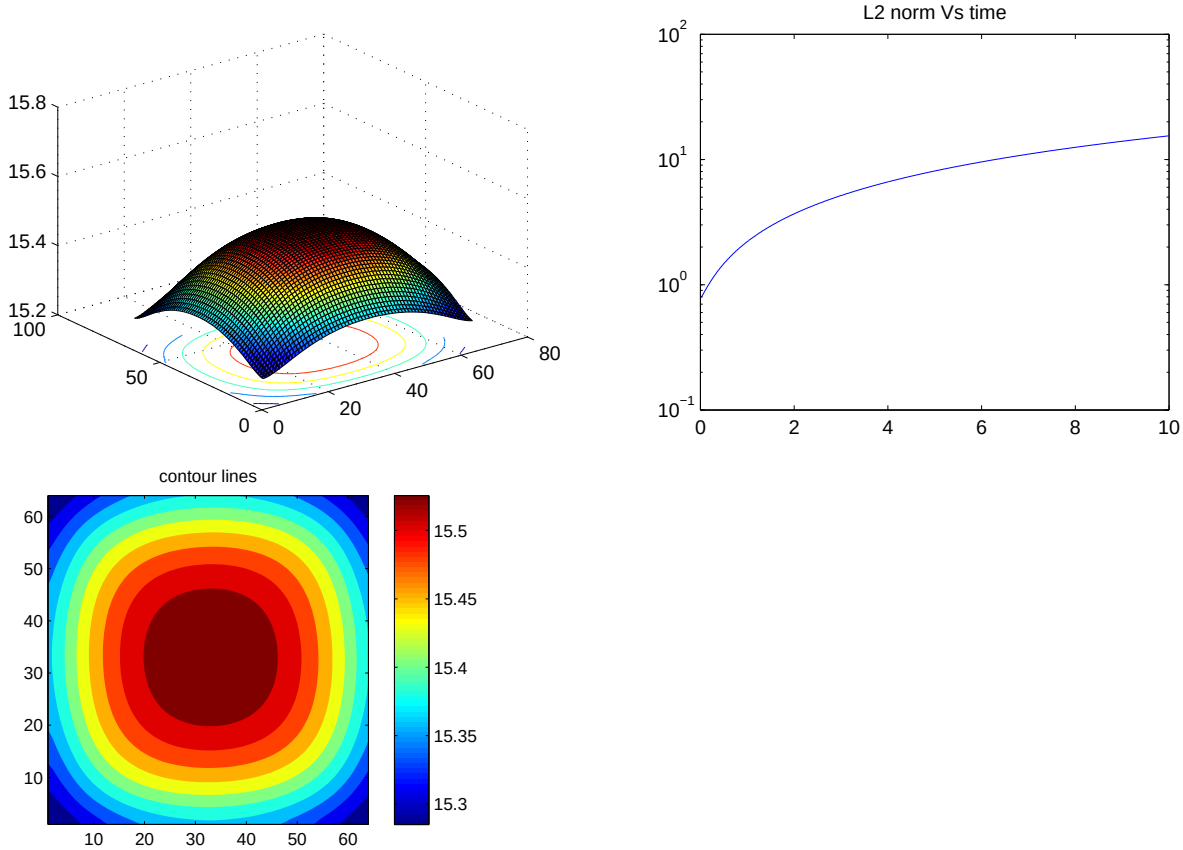

Figure 11: Global existence starting from an L^2 initial data θ^0, with $f = 2\theta_0$ and $\alpha = 0.5$ according to a full implicit Euler scheme.

From now on, we focus on the numerical simulations of the generalized quasi-geostrophic equation, for $\beta \in]0, 2\pi[\backslash k\pi$. In particular, we aim first to confirm the theoretical predictions of Section 2, and then to catch the real limitation of each parameter to get the blow-up criteria.

4.3 Numerical simulations for (GSQG)

In the sequel, we plot numerical tests, for several values of α, ν and β, and the results are illustrated by the next tables. We denote by "Y" the case when the solution blows-up, and by "N" the case when not. We also mention that the tables are arranged in the decreasing order according to the viscosity parameter ν which was arbitrary chosen in the set 1, 0.7, 0.5, 0.2, 10^{-1}, 10^{-2}, 10^{-3}, 10^{-4}. The tables prove the closure interaction between the different parameters, to give the final behavior of the solution.
For these simulations we used the linearized third order Runge-Kutta method given by Driscoll in [13] for the time discretization, and the pseudo-spectral one for the space discretization.

Remark 4 *We emphasize that all results obtained according to the Runge-Kutta scheme were already detected for the forward Euler scheme or the Splitting scheme for instance, and that this choice is done only for sake of precision to depict the exact blow-up time.*

Remark 5 *We restricted our simulations to the range $\beta \in [0, \frac{\pi}{2}]$, since we have remarked that blow-up is function of $\sin\beta$, (this will be discussed in details later).*

β \ α	0.1	0.15	0.2	0.25	0.3	0.35	0.4	0.5	0.8	1
0	N	N	N	N	N	N	N	N	N	N
$\frac{\pi}{100}$	N	N	N	N	N	N	N	N	N	N
$\frac{\pi}{10}$	N	N	N	N	N	N	N	N	N	N
$\frac{\pi}{6}$	N	N	N	N	N	N	N	N	N	N
$\frac{\pi}{4}$	Y	N	N	N	N	N	N	N	N	N
$\frac{\pi}{3}$	Y	N	N	N	N	N	N	N	N	N
$\frac{\pi}{2}$	Y	N	N	N	N	N	N	N	N	N

Table 1: $\nu = 1,\ \tau = 10^{-4}$

β \ α	0.1	0.15	0.2	0.25	0.3	0.35	0.4	0.5	0.8	1
0	N	N	N	N	N	N	N	N	N	N
$\frac{\pi}{100}$	N	N	N	N	N	N	N	N	N	N
$\frac{\pi}{10}$	N	N	N	N	N	N	N	N	N	N
$\frac{\pi}{6}$	N	N	N	N	N	N	N	N	N	N
$\frac{\pi}{4}$	Y	Y	N	N	N	N	N	N	N	N
$\frac{\pi}{3}$	Y	Y	N	N	N	N	N	N	N	N
$\frac{\pi}{2}$	Y	Y	N	N	N	N	N	N	N	N

Table 2: $\nu = 0.7,\ \tau = 10^{-4}$

β \ α	0.1	0.15	0.2	0.25	0.3	0.35	0.4	0.5	0.8	1
0	N	N	N	N	N	N	N	N	N	N
$\frac{\pi}{100}$	N	N	N	N	N	N	N	N	N	N
$\frac{\pi}{10}$	Y	N	N	N	N	N	N	N	N	N
$\frac{\pi}{6}$	Y	Y	N	N	N	N	N	N	N	N
$\frac{\pi}{4}$	Y	Y	N	N	N	N	N	N	N	N
$\frac{\pi}{3}$	Y	Y	Y	N	N	N	N	N	N	N
$\frac{\pi}{2}$	Y	Y	Y	N	N	N	N	N	N	N

Table 3: $\nu = 0.5,\ \tau = 10^{-4}$

β \ α	0.1	0.15	0.2	0.25	0.3	0.35	0.4	0.5	0.8	1
0	N	N	N	N	N	N	N	N	N	N
$\frac{\pi}{100}$	N	N	N	N	N	N	N	N	N	N
$\frac{\pi}{10}$	Y	Y	Y	Y	Y	N	N	N	N	N
$\frac{\pi}{6}$	Y	Y	Y	Y	Y	N	N	N	N	N
$\frac{\pi}{4}$	Y	Y	Y	Y	Y	N	N	N	N	N
$\frac{\pi}{3}$	Y	Y	Y	Y	Y	N	N	N	N	N
$\frac{\pi}{2}$	Y	Y	Y	Y	Y	N	N	N	N	N

Table 4: $\nu = 0.2,\ \tau = 10^{-4}$

β \ α	0.1	0.15	0.2	0.25	0.3	0.35	0.4	0.5	0.8	1
0	N	N	N	N	N	N	N	N	N	N
$\frac{\pi}{100}$	N	N	N	N	N	N	N	N	N	N
$\frac{\pi}{10}$	Y	Y	Y	Y	Y	Y	N	N	N	N
$\frac{\pi}{6}$	Y	Y	Y	Y	Y	Y	N	N	N	N
$\frac{\pi}{4}$	Y	Y	Y	Y	Y	Y	N	N	N	N
$\frac{\pi}{3}$	Y	Y	Y	Y	Y	Y	N	N	N	N
$\frac{\pi}{2}$	Y	Y	Y	Y	Y	Y	N	N	N	N

Table 5: $\nu = 10^{-1},\ \tau = 10^{-3}$

β \ α	0.1	0.15	0.2	0.25	0.3	0.35	0.4	0.5	0.6	0.7	0.8	1
0	N	N	N	N	N	N	N	N	N	N	N	N
$\frac{\pi}{100}$	N	N	N	N	N	N	N	N	N	N	N	N
$\frac{\pi}{10}$	Y	Y	Y	Y	Y	Y	Y	Y	N	N	N	N
$\frac{\pi}{6}$	Y	Y	Y	Y	Y	Y	Y	Y	Y	N	N	N
$\frac{\pi}{4}$	Y	Y	Y	Y	Y	Y	Y	Y	Y	N	N	N
$\frac{\pi}{3}$	Y	Y	Y	Y	Y	Y	Y	Y	Y	N	N	N
$\frac{\pi}{2}$	Y	Y	Y	Y	Y	Y	Y	Y	N	N	N	N

Table 6: $\nu = 10^{-2}$, $\tau = 10^{-4}$

The criteria of blow-up detected for example for the case $\beta = \frac{\pi}{3}$, $\alpha = 0.5$ and $\nu = 10^{-2}$ is illustrated by the following figures which represents the solution' blow-up and the corresponding L^2 norm:

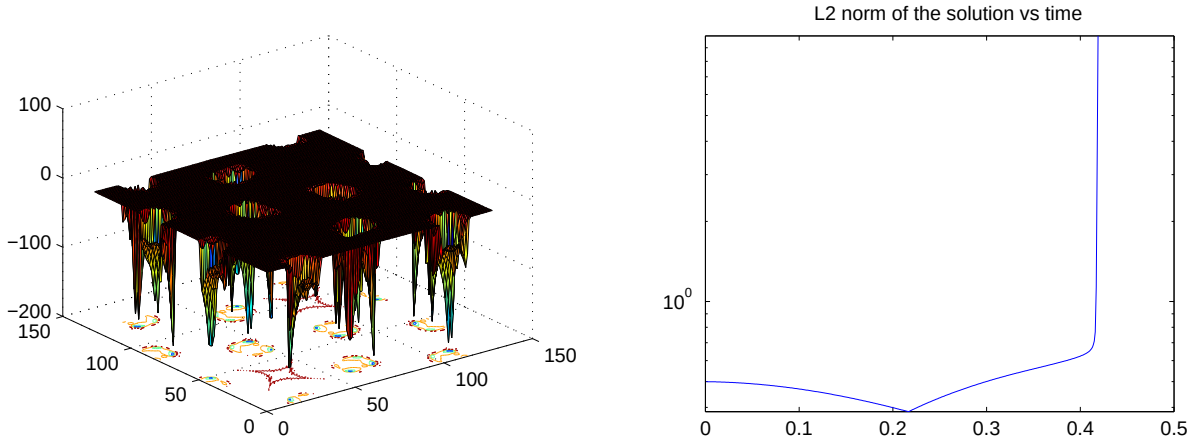

Figure 12: resolution with a third order Runge-Kutta scheme. $\alpha = 0.5$, $\nu = 10^{-2}$, $\beta = \frac{\pi}{3}$, $dx = dy = \frac{1}{128}$, $\tau = 0.0001$; $\theta^0 = \sin(2\pi x)\sin(2\pi y)$ and $f = 2\theta^0$

In [17], Dong Lie and José Rodrigo, have considered the blow-up in the supercritical range, we propose here to complete the study by considering the dissipative parameter α belonging in the whole interval $]0, 1[$; the angle $\beta \in [0 + \delta, \pi - \delta]$, where $\frac{\pi}{100} \leq \delta \leq \frac{\pi}{10}$. We emphasize that we have detected a criteria of blow up for $\beta = \frac{\pi}{100}$, for $\nu \leq 10^{-3}$. This can be observed in the following table:

β \ α	0.1	0.15	0.2	0.25	0.3	0.35	0.4	0.5	0.7	0.8	0.9	1
0	N	N	N	N	N	N	N	N	N	N	N	N
$\frac{\pi}{1000}$	Y	N	N	N	N	N	N	N	N	N	N	N
$\frac{\pi}{500}$	Y	N	N	N	N	N	N	N	N	N	N	N
$\frac{\pi}{200}$	Y	N	N	N	N	N	N	N	N	N	N	N
$\frac{\pi}{100}$	Y	Y	Y	Y	Y	N	N	N	N	N	N	N
$\frac{\pi}{10}$	Y	Y	Y	Y	Y	Y	Y	Y	Y	N	N	N
$\frac{\pi}{6}$	Y	Y	Y	Y	Y	Y	Y	Y	Y	Y	N	N
$\frac{\pi}{4}$	Y	Y	Y	Y	Y	Y	Y	Y	Y	Y	N	N
$\frac{\pi}{3}$	Y	Y	Y	Y	Y	Y	Y	Y	Y	Y	N	N
$\frac{\pi}{2}$	Y	Y	Y	Y	Y	Y	Y	Y	Y	N	N	N

Table 7: $\nu = 10^{-3}$, $\tau = 10^{-4}$

β \ α	0.1	0.15	0.2	0.25	0.3	0.35	0.4	0.5	0.8	0.9	0.95	1
0	N	N	N	N	N	N	N	N	N	N	N	N
$\frac{\pi}{1000}$	Y	Y	Y	Y	Y	Y	Y	Y	N	N	N	N
$\frac{\pi}{500}$	Y	Y	Y	Y	Y	Y	Y	Y	Y	N	N	N
$\frac{\pi}{200}$	Y	Y	Y	Y	Y	Y	Y	Y	Y	Y	N	N
$\frac{\pi}{100}$	Y	Y	Y	Y	Y	Y	Y	Y	Y	Y	Y	N
$\frac{\pi}{10}$	Y	Y	Y	Y	Y	Y	Y	Y	Y	Y	Y	N
$\frac{\pi}{6}$	Y	Y	Y	Y	Y	Y	Y	Y	Y	Y	Y	Y
$\frac{\pi}{4}$	Y	Y	Y	Y	Y	Y	Y	Y	Y	Y	Y	Y
$\frac{\pi}{3}$	Y	Y	Y	Y	Y	Y	Y	Y	Y	Y	Y	Y
$\frac{\pi}{2}$	Y	Y	Y	Y	Y	Y	Y	Y	Y	Y	Y	N

Table 8: $\nu = 10^{-4}$, $\tau = 10^{-5}$

Remark 6

- *Notice that the criteria of blow-up simulated in the previous tables is independent of the choice of the time step τ particularly, we implemented all the tests of Table7 for example, with $\tau = 10^{-3}$ or $\tau = 10^{-5}$ and the results were unchanged.*

- *Besides, the criteria of blow-up is closely related to the L^2 norm of the initial data θ^0. Hence, this test confirm one more time the theoretical predictions, which pretend that under some smallness conditions on the initial data's norm, we can prove global existence of the solution of (1).*

  We specify that we implemented several tests where the solution blew-up in finite time for an initial data θ^0 and didn't for $\frac{\theta^0}{2}$.

The non blow-up in the case $\alpha = 1$ is illustrated by a convergence to a stationary solution detected on the L^2 norm. This can be observed in the following figure which corresponds to the evolution of

the L^2 norm of the solution to the (GSQG) equation with $\beta = \frac{\pi}{2}$ and $\nu = 10^{-4}$ for instance.

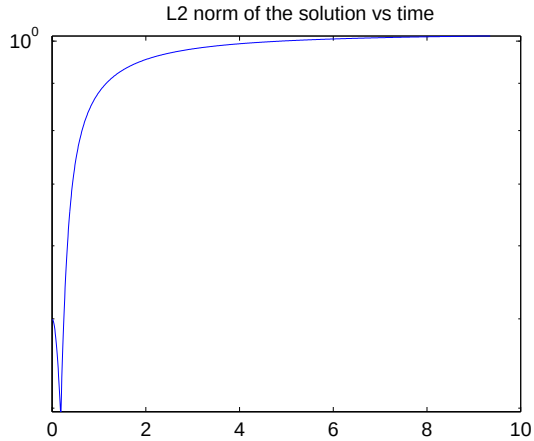

Figure 13: resolution with a third order Runge-Kutta code. $\alpha = 1$, $\nu = 10^{-4}$, $\beta = \frac{\pi}{2}$, $dx = dy = \frac{1}{128}$, $\tau = 0.0001$; $\theta^0 = \sin(2 * \pi * x)\sin(2 * \pi y)$ and $f = 2\theta^0$

4.4 Toward the capture of a law for the blow-up

Let us denote by T^* the blow-up time which can be estimated by the numerical simulations for fixed diffusion and viscosity parameters α and ν. It is then easy to observe that T^* is an increasing function of the decreasing rate of $\sin\beta$. Particularly, the limiting criteria of non blow-up for $\beta = k\pi$ enforced these predictions, and $T^* = \phi(\frac{1}{\sin\beta})$ seems to be a good apprehension.
However, to more understand the variation of this blow-up time, according to the different parameters, we draw some tables giving the blow-up time T^*, respectively by fixing two parameters and varying the third one of them. More precisely, the Table(9), Table(10), Table(11) and Table(12) give the resulting blow-up time with respect to β for respective fixed α and ν. We confirm by these tables that the blow-up time is an increasing function of ν.

β	$\frac{\pi}{10}$	$\frac{\pi}{9}$	$\frac{\pi}{8}$	$\frac{\pi}{7}$	$\frac{\pi}{6}$	$\frac{\pi}{5}$	$\frac{\pi}{4}$	$\frac{\pi}{3}$	$\frac{7\pi}{20}$	$\frac{2\pi}{5}$	$\frac{\pi}{2}$
T^*	N		1.79	1.27	1.02	0.82	0.66	0.53	0.52	0.48	0.51

Table 9: $\nu = 0.5,\ \alpha = 0.15$

β	$\frac{\pi}{10}$	$\frac{\pi}{9}$	$\frac{\pi}{8}$	$\frac{\pi}{7}$	$\frac{\pi}{6}$	$\frac{\pi}{5}$	$\frac{\pi}{4}$	$\frac{\pi}{3}$	$\frac{7\pi}{20}$	$\frac{2\pi}{5}$	$\frac{\pi}{2}$
T^*	0.91	0.84	0.75	0.68	0.61	0.54	0.47	0.41	0.4	0.37	0.38

Table 10: $\nu = 10^{-1},\ \alpha = 0.1$

β	$\frac{\pi}{10}$	$\frac{\pi}{9}$	$\frac{\pi}{8}$	$\frac{\pi}{7}$	$\frac{\pi}{6}$	$\frac{\pi}{5}$	$\frac{\pi}{4}$	$\frac{\pi}{3}$	$\frac{7\pi}{20}$	$\frac{2\pi}{5}$	$\frac{\pi}{2}$
T^*	0.86	0.79	0.71	0.65	0.59	0.52	0.46	0.4	0.39	0.37	0.37

Table 11: $\nu = 10^{-2},\ \alpha = 0.25$

β	$\frac{\pi}{10}$	$\frac{\pi}{9}$	$\frac{\pi}{8}$	$\frac{\pi}{7}$	$\frac{\pi}{6}$	$\frac{\pi}{5}$	$\frac{\pi}{4}$	$\frac{\pi}{3}$	$\frac{7\pi}{20}$	$\frac{2\pi}{5}$	$\frac{\pi}{2}$
T^*	0.85	0.78	0.7	0.64	0.58	0.52	0.45	0.39	0.38	0.36	0.37

Table 12: $\nu = 10^{-3},\ \alpha = 0.35$

On the other hand, since we have simulated the results for various α, we opted for two other kinds of studies, fixing separately α and ν, to depict the accurate influence of both diffusion and viscosity parameters on T^*. The results are given in tables (13) and (14) for fixed ν and β, and in Table (15) for fixed α. We emphasize that all the following simulations are resulting from an implementation of the Runge-Kutta scheme for $\tau = 10^{-4}$ and $N = 128$:

α	0.1	0.15	0.2	0.25	0.3	0.35
T^*	0.45	0.45	0.45	0.45	0.46	0.46

Table 13: $\nu = 10^{-2},\ \beta = \frac{\pi}{4}$

α	0.1	0.15	0.2	0.25	0.3	0.35
T^*	0.58	0.58	0.58	0.58	0.58	0.59

Table 14: $\nu = 10^{-2},\ \beta = \frac{\pi}{6}$

Obviously, the blow-up time seems to depend more on the viscosity parameter ν than on the diffusion parameter α for fixed β. Indeed, for fixed α we get:

β	$\frac{\pi}{2}$	$\frac{2\pi}{5}$	$\frac{7\pi}{20}$	$\frac{\pi}{3}$	$\frac{\pi}{4}$
$T^*_{\nu_1}$	0.39	0.38	0.4	0.42	0.48
$T^*_{\nu_2}$	0.51	0.48	0.52	0.53	0.66
$T^*_{\nu_3}$	0.67	0.59	0.65	0.68	0.96

Table 15: $\nu_1 = 10^{-1},\ \nu_2 = 0.5,\ \nu_3 = 0.7,\ \alpha = 0.15$

We observe from the previous table, that the variation of the blow-up time owing to a variation $\nu_i \leftrightarrow \nu_j$ depends also on β.
All of these numerical observations let us expect that the blow-up time can be written as:

$$T^* = a * \frac{1}{(\sin\beta)^{\varphi(\nu)}}$$

where a depends on ν and α, and φ is some function of ν. Indeed, the following graphs confirm this deduction.

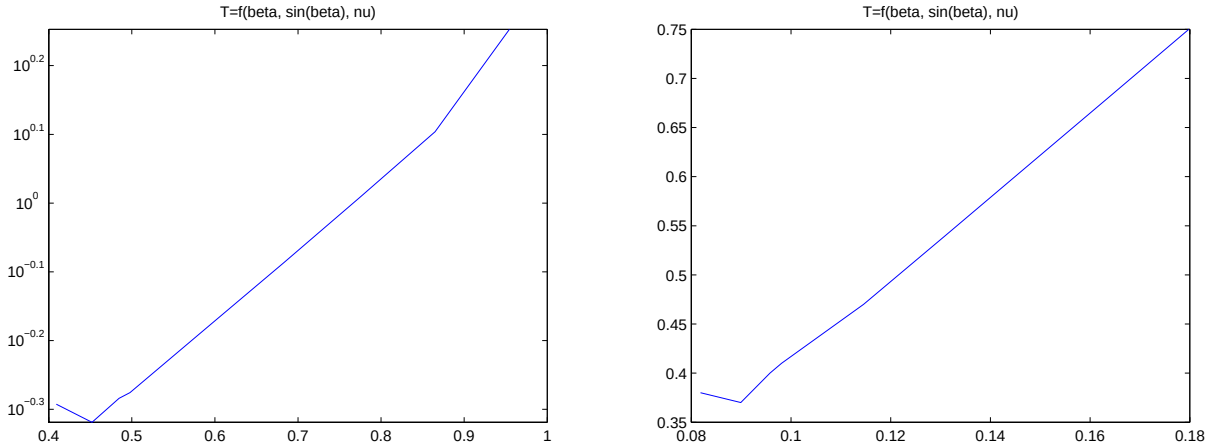

Figure 14: Blow-up time first for $\alpha = 0.15$ and $\nu = 0.5$ and second for $\alpha = 0.1$ and $\nu = 0.1$ according to the Runge-Kutta scheme.

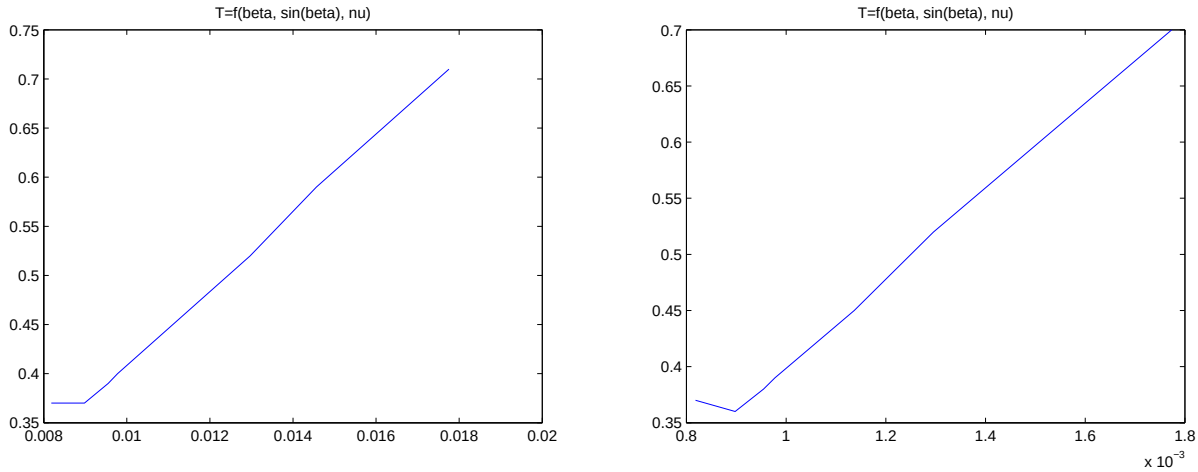

Figure 15: Blow-up time first for $\alpha = 0.25$ and $\nu = 0.01$ and second for $\alpha = 0.35$ and $\nu = 0.001$ according to the Runge-Kutta scheme.

These graphs correspond precisely to the blow-up function:

$$T^* \simeq \frac{\nu}{2} \frac{1}{(\sin\beta)^{\frac{\nu}{2}}} + b.$$

Besides, due to the fact that for $\alpha = 1$ we depicted an infinite blow-up time, than we concluded that the blow-up time can be fitted by a band given by:

$$\phi_{up} = \frac{\nu}{2(1-\alpha)} \frac{1}{(\sin\beta)^{\frac{\nu}{2}}} + b \tag{65}$$

$$\phi_{sub} = \frac{1}{(1-\alpha)} \frac{1}{(\sin\beta)^{\frac{\nu}{2}}} + b. \tag{66}$$

The results are given by the following figures:

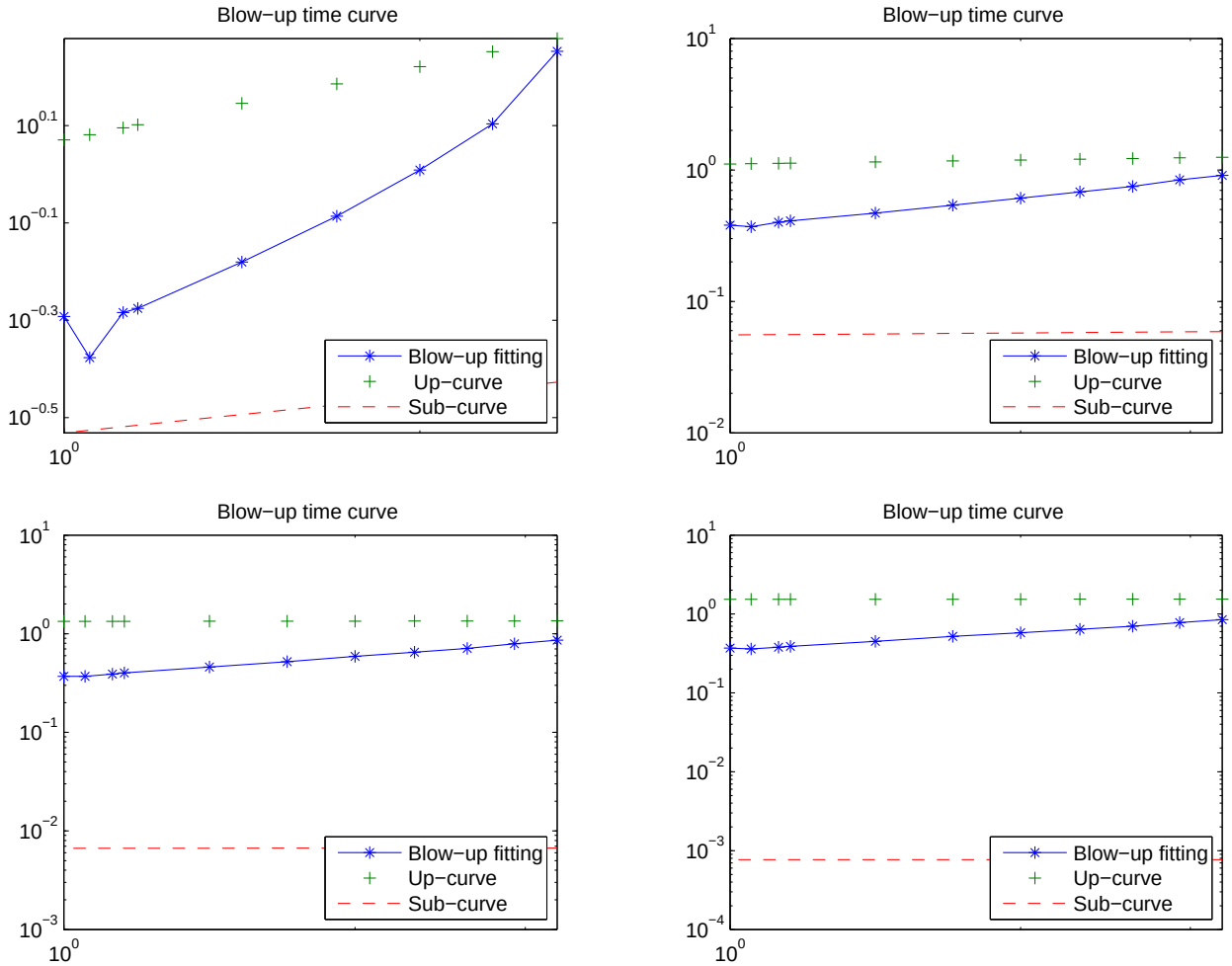

The major question that we have to answer now is to get some formula which control this blow-up, that depend on several parameters.Let us define at first, the discrete H^α norm given by

$$\| \theta \|_{N,\alpha}^2 = \| (-\Delta)^{\frac{\alpha}{2}} \theta \|_{N,2}^2 = \frac{1}{N^2} \sum_{i=1}^{N} \sum_{j=1}^{N} | (-\Delta)^{\frac{\alpha}{2}} \theta_{i,j} | .$$

Since the blow-up is happened at the rate of $\| \theta \|_{H^\alpha}$, (as showed in figure (16)) we suppose that the quantity

$$\eta(t) = \| \theta^N(.,t) \|_{H^\alpha} \tag{67}$$

is known at different times t_i, and that the blow-up time T^* is numerically known,

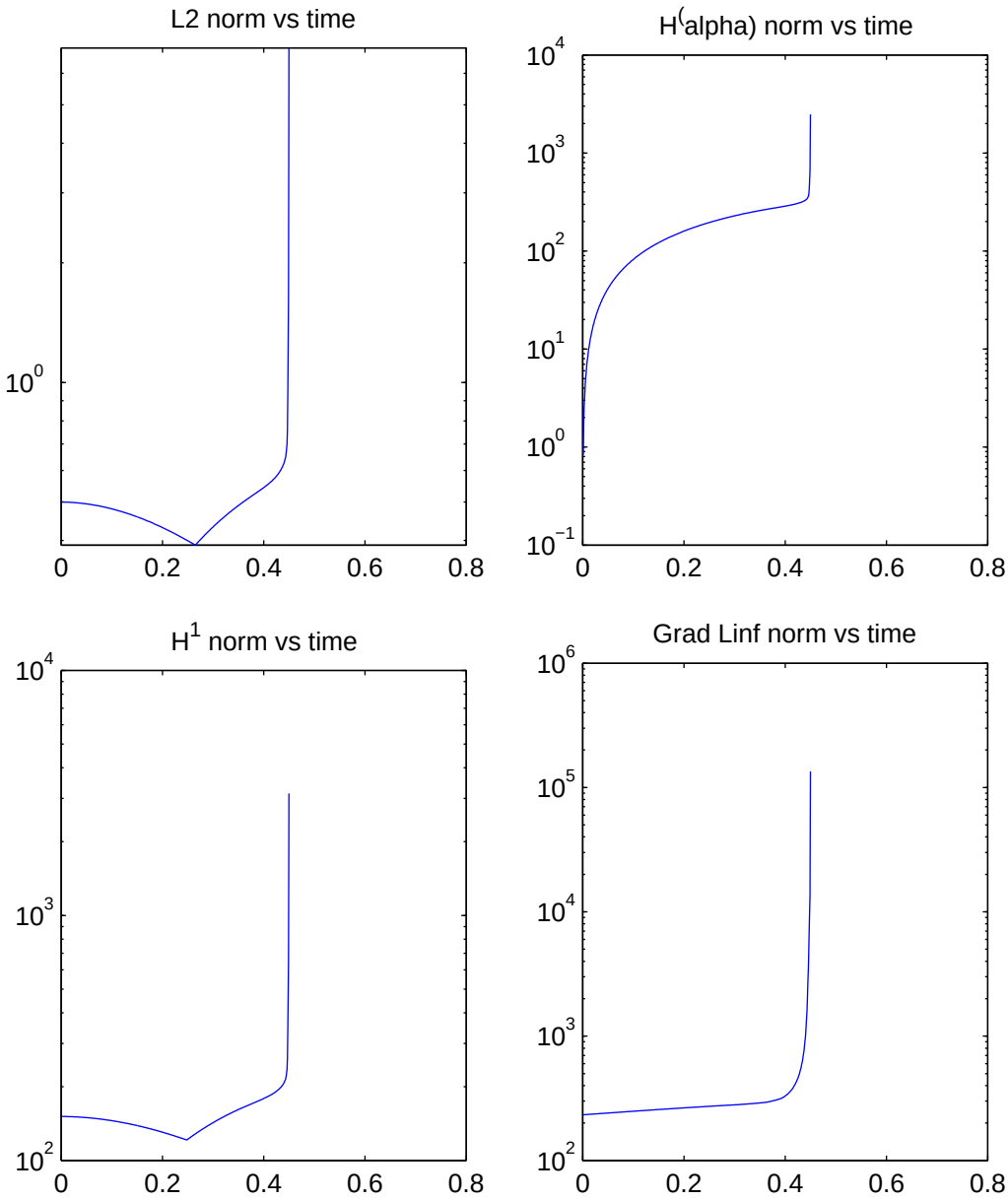

Figure 16: The blow-up according to each norm

then, we have to compare the rapid growth rates in the solutions norm with different predictable laws, for times close to the blow-up time T^*. The resulting graphs according first to an exponential type law

$$\eta_1(t) = \exp(T^* - t)^{-1},$$

and second to an empirical asymptotic fitting law,

$$\eta_2(t) = (T^* - t)^{-1},$$

are shown in Figure 14 and Figure 15.

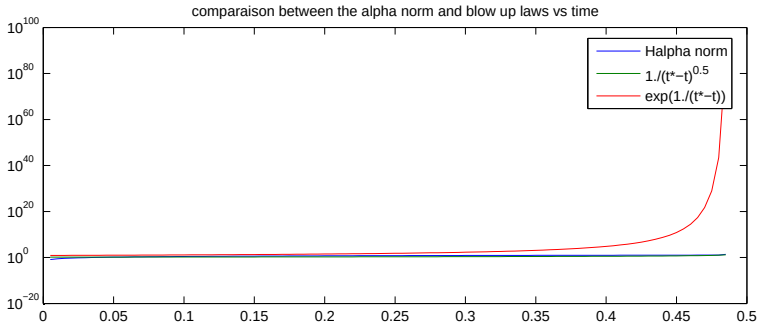

Figure 17: A comparaison between the exponential blow-up law $\eta_1(t)$ and the solution' H^α norm Vs time, for $\alpha = 0.5$, $\beta = \frac{\pi}{4}$, $\nu = 10^{-2}$, $dt = 10^{-4}$, $N = 128$.

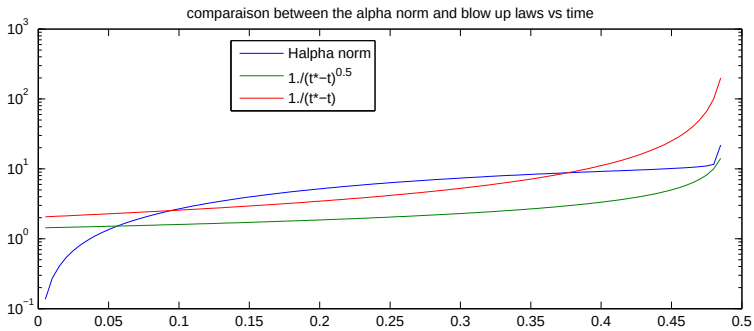

Figure 18: A comparaison between the hyperbolic blow-up law $\eta_2(t)$ and the solution' H^α norm Vs time, for $\alpha = 0.5$, $\beta = \frac{\pi}{4}$, $\nu = 10^{-2}$, $dt = 10^{-4}$, $N = 128$.

These numerical observations, let deduce that the norm growth here is less rapid than the two predicted laws, and give reason to an asymptotic fitting

$$\eta(t) = C(\alpha, \beta, \nu)(T^* - t)^{-\gamma}.$$

A second set of numerical computations, shows that the fitted mean square rate γ decreases according to α, $\sin\beta$ and ν as shown in the following tables:

β \ α	0.15	0.25	0.35	0.5	0.6
$\frac{\pi}{4}$	0.2967	0.2467	0.2144	0.1733	0.1437
$\frac{\pi}{6}$	0.0262	0.2603	0.2202	0.1775	0.1331

Table 16: The fitted slope γ for $\nu = 10^{-2}$

β \ α	0.15	0.25	0.35	0.5	0.6
$\frac{\pi}{4}$	0.2989	0.2485	0.2137	0.0263	0.1588
$\frac{\pi}{6}$	0.3220	0.0264	0.2253	0.1830	0.1636

Table 17: The fitted slope γ for $\nu = 10^{-3}$

Hence, for a, b, c some positive reals, the rate γ can be expected equal to:

$$\gamma = a(1-\alpha) + b(1-\sin\beta) + c(1-\nu).$$

5 Conclusion

We performed numerical computations on the asymptotic behavior of solutions to (SQG) and (GSQG) equations. Theory and experiments agree: the solution of the usual (SQG) globally exists for a dissipation $\alpha \geq \frac{2}{3}$, and moreover beyond the range $\alpha \in [\frac{1}{2},\ 1[$, which implies that the theoretical limitations are only technical, and that there is no critical behavior at $\alpha = \frac{1}{2}$.

In the case of (GSQG), solutions blow-up on $\mathbb{T}^2$ for the whole range $\alpha \in\ ]0,\ 1[$, according to an explicit formula which controls the time blow-up, depending on sin β, $\frac{1}{1-\alpha}$,, and ν. The question of capturing a precise law of blow up with these parameters is still open; the method we have presented here and which consists in tabuling the blow-up situations according to the values of teh different parameters offers a way to approach the rate of blow-up, using approximation techniques.

Acknowledgments

This paper was partially supported by the "MASOH" project, and the most important part of the work was achieved during multiple stays of the second author in the LAMFA/UPJV in Amiens with support of the INRIA under "CO-ADVISE" project.

References

[1] P. Balodis, A. Còrdoba, Inequality for Riesz transforms implying blow-up for some nonlinear and nonlocal transport equations, Adv. Math. 214(1), 1-39(2007).

[2] L. Berselli, Vanishing viscosity limit and long-time behavior for 2D quasigeostrophic equations, Indiana Univ.Math.J. 51, No.4,905-930(2002).

[3] L. Caffarelli, A. Vasseur, Drift diffusion equation with fractional diffusion and the quasi-geostrophic equation, Ann. of. Mat (2) 171 (2010), nà. 3, 1903-1930.

[4] D. Cahe, J. Lee, Global well posedness in the supercritical dissipative quasigeostrophic equations, Comm. Math. Phys. 233(2003) 297-311.

[5] J. A. Carrillo, L. C. F. Ferreira, The asymptotic behavior for the subcritical dissipative quasi geostrophic equations Nonlinearity 21 (2008), no. 5, 1001-1018.

[6] J. P. Chehab, M. M. Trabelsi and E. Zahrouni, On a discretization in time of a 2D dissipative Quasi Geostrophic equation, Submittted

[7] P. Constantin, D. Cordoba and J. Wu. On the critical dissipative quasi-geostrophic equation. Indiana Univ. Math. J., 50 Spec. Iss.: 97–107 (2001).

[8] P. Constantin, Q. Nie and N. Schorghofer, Nonsingular surface quasi geostrophic flow, Phys. Lett. A 241 (1998), 168-172.

[9] P. Constantin, J. Wu, Behavior of solutions of 2D quasi geostrophic equations, SIAM J. Math. Anal., 30(1999) 937- 948.

[10] A. Cordòba, D. Còrdoba, A maximum principle applied to quasi geostrophic equations. Comm. Math. Phys. 249(2004) 511-528.

[11] H. Dong, D. Li, Finite time singularities for a class of generalized surface quasi geostrophic equations, Proc. Amer. Math. Soc. 136, 2555-2563(2008).

[12] H. Dong, D. Li, Spatial analicity of the solutions to the sub-critical dissipative quasi geostrophic equations, Arch. Ration. Mech. Anal. 189 (2008), no 1.

[13] Tobin A. Driscoll, A composite Runge-Kutta method for the spectral solution of semilinear PDEs. Journal of Computational physics 182, 357–367(2002).

[14] N. Ju, Dissipative quasi geostrophic equation: local well-posedness, global regularity and similarity solutions, Indiana univ. Math. J. 56, (2007), no. 1,187–206.

[15] N. Ju. The maximum principle and the global attractor for the dissipative 2D quasi-geostrophic equations, Comm. Math. Phys., 255 (2005) 161Ű-181.

[16] H. Kalisch, J.L. Bona, Singularity formation in the generalized Benjamin-Ono equation, Discrete and continuous dynamical systems, Vol 11, Number 1, July (2004), pp 27-45.

[17] D. Li and J. Rodrigo. Blow Up for the Generalized Surface Quasi-Geostrophic Equation with Supercritical Dissipation, Commun. Math. Phys., 286, (2009), 111Ű-124, (2009).

[18] A.J. Majda, E.G. Tabak, A two-dimensional model for quasi-geostrophic flow: comparison with the two-dimensionalEuler Flow, Physica D.98 (1996), 515-522.

[19] K. Ohkitani, M. Yamada, Inviscid and Inviscid-limit behavior of a surface quasigeostrophic flow, Phys. Fluids 9 (1997), 876-882.

[20] S. Resnick, *Dynamical problems in Non-linear Advances Partial Differential Equations,* Ph.D. thesis, University of Chicago, II, 1995.

[21] R. Temam, *Infinite Dimensional Dynamical Systems in Mechanics and Physics,* Springer-Verlag, Second Edition, (1997).

[22] M. M. Trabelsi, *Equations quasigéostrophiques : systèmes dynamiques et simulation,* PhD Thesis, FSM Monastir, October 2012.

[23] M.M. Trabelsi and E. Zahrouni, Dynamical system of a second order discretization in time of a 2D dissipative Quasi Geostrophic equation, Preprint (2009).

[24] J. Wu Global solutions of the 2D dissipative quasi-geostrophic equation in Besov spaces, SIAM J. Math. Anal., 36 (2004-2005) 1014- 1030 .

[25] J.Wu. Existence and uniqueness results for the 2D dissipative quasi-geostrophic equations, Nonlinear analysis, 67(2007) 3013-3036 .

[26] J. Wu Global solutions of the 2D dissipative quasi-geostrophic equation in Besov spaces, SIAM J. Math. Anal., 36(2004-2005) 1014- 1030 .

[27] J.Wu. Existence and uniqueness results for the 2D dissipative quasi-geostrophic equations, Nonlinear analysis, 67(2007) 3013-3036 .